Applications

Molecular Dynamics Simulations of Acetylcholinesterase – Beta-Amyloid Peptide Complex

Mariana Atanasova[1], Ivan Dimitrov[1], Stefan Ivanov[1,2]

[1]Faculty of Pharmacy, Medical University of Sofia, Sofia, Bulgaria
[2]Institute for Bioscience and Biotechnology Research, University of Maryland, Rockville, MD 20850, USA
E-mails: *matanasova@pharmfac.mu-sofia.bg*   *idimitrov@pharmfac.mu-sofia.bg*
sivanov@ddg-pharmfac.net

Abstract: *Alzheimer's Disease (AD) is a neurodegenerative disorder with severe consequences and lethal outcome. One of the pathological hallmarks of the disease is the formation of insoluble intercellular beta-Amyloid (Aβ) plaques. The enzyme ACetylcholinEsterase (AChE) promotes and accelerates the aggregation of toxic Aβ protofibrils progressively converted into plaques. The Peripheral Anionic Site (PAS), part of the binding gorge of AChE, is one of the nucleation centers implicated in the Aβ aggregation. In this study, the Aβ peptide was docked into the PAS and the stability of the formed complex was investigated by molecular dynamics simulation for 1 μs (1000 ns). The complex was stable during the simulation. Apart from PAS, the Aβ peptide makes several additional contacts with AChE. The main residence area of Aβ on the surface of AChE is the region 344-361. This region is next to PAS but far enough to be sterically hindered by dual-site binding AChE inhibitors.*

Keywords: *Alzheimer's disease, beta-Amyloid (Aβ), acetylcholinesterase (AChE), Peripheral Anionic Site (PAS), Aβ aggregation, senile plaques, amyloid fibrils, neurodegenerative disorder, molecular dynamics.*

1. Introduction

Amyloidogenic proteins are group of proteins that undergo conformational changes leading to amyloid fibril formation and causing diseases [1]. Such known proteins are transthyretin in senile systemic amyloidosis and in familial amyloid polyneuropathy I, prion in spongyform encephalopathies, islet amyloid polypeptide in type II diabetes, β-Amyloid (Aβ) peptide in Alzheimer's Disease (AD) [1]. A common feature of many neurodegenerative disorders is amyloidosis, abnormal protein aggregation forming insoluble extracellular fibrils [2]. The most widespread

and affecting tens of millions of elderly people dementia is AD, a progressive and irreversible disorder [3]. It is characterized with gradual memory loss and cognitive dysfunction. Both forms of AD – a familial, caused by mutations in some certain genes, and non-familial, the vast majority of cases, with unknown aetiology and occurring sporadically [4] – share common neuropathological features. These are the extracellular Senile Plaques (SPs) formed by deposition of beta-amyloid peptides and other proteins and the intracellular neurofibrillary tangles of abnormally phosphorylated tau protein in the brain [5]. The major protein of SPs is Aβ peptide which is generated intracellularly via sequential proteolysis by β- and γ-secretase within the Amyloid Precursor Protein (APP) [6-8]. Multiple Aβ alloforms of different lengths are derived due to variations in the performance of γ-secretase [9, 10]. Among them, peptides with length 1-39, 1-40, 1-41, 1-42 and 1-43 have been identified as the major components of the amyloid deposits [11]. The amyloidogenic process is associated with active structural changes at the secondary structure of Aβ peptide at which non-pathogenic α-helical soluble conformation transits to β-strand structure capable to assemble into insoluble amyloid fibrils [11-14]. These conformational states are maintained by the peptide monomer itself, the density of oligomer and the sequence of events leading to amyloidosis [15]. Currently, it is considered that fibrillization is a nucleation-dependent process, resembling in some extend crystallization, that can be altered by different physicochemical factors and promoted by the presence of "a seed" [11, 12]. Among the several macromolecules reported to be associated with senile plaques like apolipoprotein E, α$_1$-antichymotrypsin, α$_2$-macroglobulin, heptaglobin, laminin, complement factors, clusterin, perlecan and ACetylcholinEsterase (AChE) [16-22], apolipoprotein E, α$_1$-antichymotrypsin and AChE are identified as "Aβ pathological chaperons" as they have ability to promote amyloidosis [17, 19, 23, 24].

AChE (EC 3.1.1.7) has received much attention according to its dual functionality – the classic catalytic or cholinergic and non-cholinergic manifested in the central and peripheral nervous system [25-27]. The catalytic function is related to rapid hydrolysis of the neurotransmitter ACetylcholine (ACh), breaking it into choline and acetate and thus the cholinergic transmission is terminated [28]. Currently, the symptomatic treatment of AD is based on the cholinergic activity of the enzyme. It consists of controlled inhibition of AChE, which enhances the acetylcholine levels that are usually depleted in AD patients. Thus, the transmission of cholinergic synapses is ameliorated which results in improved cognitive function. Much research interest is focused on the non-cholinergic manifestations of the enzyme associated with a possible role of development of AD [18, 29]. AChE has been discovered in preamyloid diffuse deposits, mature SPs and cerebral blood vessels [12, 30]. As it was mentioned above, AChE serves as a "chaperone" in amyloid formation promoting the assembly of Aβ and enhancing the Aβ association, deposition and fibril formation [23, 24, 31, and 32]. Furthermore it has been found that complexes of AChE-Aβ are more toxic than those Aβs aggregated alone [33]. The Peripheral Anionic Site (PAS), consisted of aromatic amino acids and located at the entrance of the binding gorge of AChE, has been recognized as a structural motif that binds the amyloid beta peptide [32]. This finding prompted to the development

of many dual-site binding AChE inhibitors – ligands that bind simultaneously to the enzyme active site and to PAS [34]. A molecular docking study of Aβ and AChE revealed several potential binding regions of the enzyme including the PAS [35]. Another N-terminal AChE$_{7-20}$ motif was discovered to implicate in Aβ aggregation and deposition [36, 37]. Recently, the state-of-the-art accelerated Molecular Dynamics (MD) simulation was performed on a system of human AChE and 10 Aβ peptides for 200 ns in order to investigate the whole surface of the enzyme and the mechanism of aggregation [38]. It was confirmed that AChE attracts and forms stable complexes with Aβ. Fifteen contact sites on the AChE surface have been identified, including the previously described N-terminal region and PAS.

In the present study we investigate the stability of a complex between a single Aβ peptide docked at the PAS of AChE via a classical atomistic MD simulation for 1 μs (1000 ns) and identify the main residence areas of Aβ on the surface of AChE.

2. Methods

2.1. Molecular docking

Crystallographic structure of human recombinant AChE (rhAChE, pdb id: 4ey6, $R = 2.40$ Å) [39] and NMR structure of Aβ peptide (pdb ID: 1aml) [40] were used as input structures for molecular docking study. Galanthamine molecule was removed from the binding site of AChE as well as all water molecules. Molecular docking was performed on RosettaDock online server [41]. The Aβ peptide was randomly positioned near the PAS of AChE.

2.2. System preparation

The best scored complex between AChE and Aβ resulted from the docking was subject to MD simulation. The protein chain was capped at each end and at the ends of broken parts (residues 259, 262, 492 and 495). The system was protonated and solvated in a truncated octahedral box with TIP3P water [42]. Physiological salt concentration was provided adding NaCl to ensure neutrality of the system. The final system consists of over 76 000 atoms.

2.3. Molecular dynamics

Initially the solvated system was energy minimized for 2000 steps with harmonic restraints of 3 kcal/molÅ^2 on protein and peptide heavy atoms. Next, the system was heated from 0 to 300 K over 1 ns with identical restrains, followed by 1 ns of constant pressure density equilibration with restraints. Then, the system was equilibrated for 1 ns without any restrains. The equilibrated system was subject to 1000 ns of production dynamics under constant temperature (300 K) and pressure (1 bar), provided with the Langevin thermostat [43] and Berendsen barostat [44], respectively. The ff14SB force field [45] was used for the system simulation as periodic boundary conditions were applied. A 12.0 Å cutoff was used for both van der Waals and electrostatic interactions; long-range electrostatics beyond the real-space cutoff were evaluated with the Particle-Mesh Ewald (PME) scheme [46].

During heating, density equilibration, preproduction, and production dynamics, covalent bonds to hydrogen were constrained using the SHAKE Algorithm [47], allowing for a 2 fs time step; only during energy minimization bonds to hydrogen were not constrained. During production dynamics, frames were saved every 0.2 ns for a total of 5000 per trajectory, to be used in subsequent analysis. The trajectory analyses were performed by cpptraj V4.14.0 [48]. The Gromacs rdf tool was used for generation the Radial Distribution Functions (RDFs) around the peptide.

3. Results and discussion

The best scored pose of the by AChE-Aβ complex predicted by RosettaDock is shown in Fig. 1A, Appendix. The peptide is located at the rim of AChE binding gorge and its N-terminal is bound in the PAS by π-π stacking between Phe4 of Aβ and Trp286 of PAS. This model was used as a starting structure for 1000 ns molecular dynamics simulations applying the protocol described in Methods. The π-π stacking between Phe4 and Trp286 was lost during the preproduction phase but the C-terminal of Aβ remains bound to PAS for the first 100 ns. In the given snapshot in 88.6 ns four hydrogen bonds are formed between the two molecules (Fig. 1B, Appendix). They are between Asp1 and Tyr341, Asp23 and Ser355, Gly25 and Arg364 and Ser26 and Arg364. A π-π stacking occurs between Phe4 and His287. A hydrophobic interaction is formed between Val39 and Ala357. Next, the C-terminal escapes from PAS (Fig. 1C, Appendix). In the given snapshot at 418.8 ns, the peptide forms five hydrogen bonds between Asp1 and Glu351, Asp1 and Leu353, Glu3 and Asn350, Glu22 and Ser355 and Ser26 and Arg364. One hydrophobic interaction occurs between Phe4 and Val365. The peptide occupies this area on the surface of AChE for around 350 ns and then moves again close to PAS (Fig. 1D, Appendix). In the given complex at 525.8 ns, six hydrogen bonds are formed: between Asp1 and Glu351, Glu3 and Asn350, His14 and Phe346, Glu15 and Ser347, Glu15 and Asp349, and Gly9 and Gly345. There is also one hydrophobic contact between His14 and Gly345. The peptide occupies this area till the end of the simulation as frequently shifts to PAS and between 702 ns and 963 ns occupies the PAS (Fig. 1E, Appendix). In the presented snapshot at 711.4 ns, seven hydrogen bonds are formed between Aβ and AChE. They are between Asp1 and Glu351, Asp1 and Leu353, Ala2 and Glu358, Glu3 and Asn350, His14 and Phe346, Gln15 and Ser347, and Gln15 and Asp349. One hydrophobic contact occurs between Phe4 and Ala361.

3.1. Complex stability

The mean values of backbone C-atoms (bb) RMSDs (root mean square deviation) over time for the complex and for the two single molecules are given in Fig. 1. Initially, the complex undergoes two transformations (at 100 ns and 300 ns) and after ~550 ns it stabilizes. The first transformation happens at around 100 ns with small changes in bb RMSDs (~1 Å) (Fig. 1A). The second transformation starts at around 400 ns and undergoes with bigger changes in bb RMSDs (~2.5 Å).
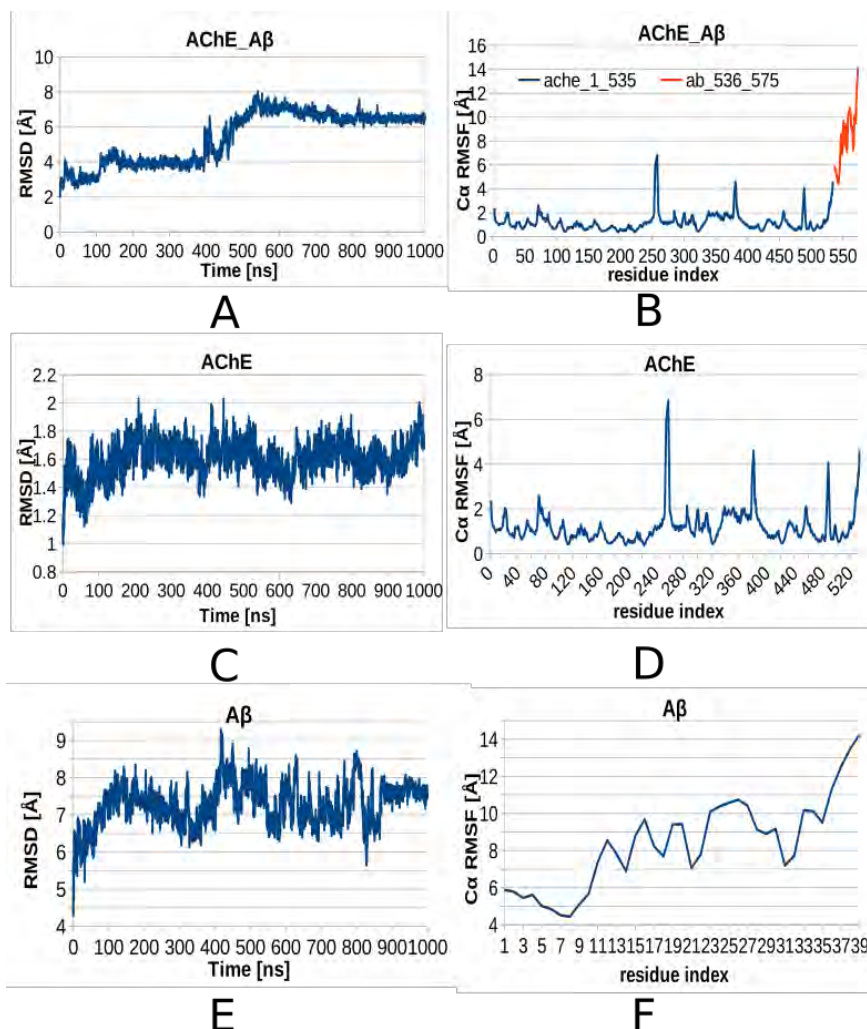
Fig. 1. Backbone C-atoms RMSDs (left graphs) and RMSFs (right graphs)
for AChE and Aβ (A and B), for AChE (C and D) and for Aβ (E and F)

The structure of the AChE is stable during the MD simulation. The averaged bb RMSDs vary below 2 Å (Fig. 1C). Not surprisingly, the small peptide molecule makes the greatest changes in bb RMSDs while it moves to fit best on the AChE surface (Fig. 1E).

The backbone root mean square fluctuations (bb RMSFs) of AChE show that the enzyme is quite stable most of the time (Fig. 1). The most fluctuating residues belong to the unstructured region between 373 and 384 positions, around the capped chain breaks at 255 and 486 positions, and to the C-terminal (Fig. 1B and D). In contrast, all residues of Aβ are highly fluctuating with RMSF values in the range 4-14 Å (Fig. 1F). Among them, the N-terminal is the most rigid – with RMSF up to 6 Å.

The Radial Distribution Function (RDF) of Aβ around AChE is given in Fig. 2A. RDF estimates the probability of a given molecule or a group to be found at a given distance from another molecule rather to be found in the bulk solvent, where its value equals 1. Values above 1 shows that the given molecule is more likely to be found around another molecule at a given distance than in the solvent. The RDF of Aβ around AChE shows that Aβ is more likely to be found around AChE within 3 Å distance rather than in the solvent. Furthermore, in order to prove the reliability of this result we separate the production dynamics trajectories into four equal parts and estimates RDF for each of them (Fig. 2B). The four RDF curves have the same shape – Aβ exists within 3 Å distance around AChE.

(A) (B)
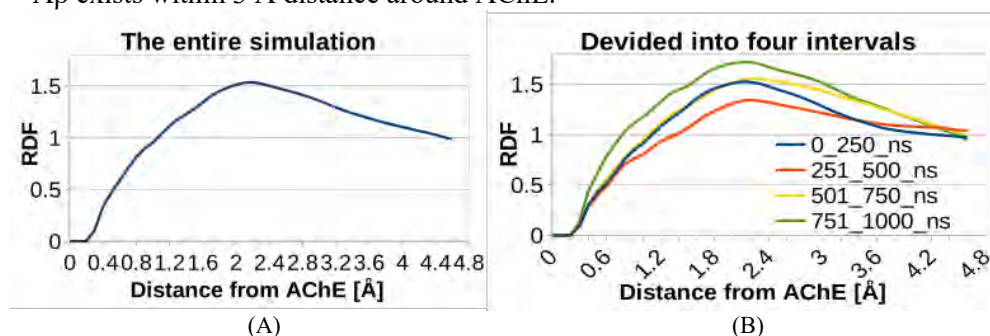
Fig. 2. Radial distribution function (RDF) of Aβ around the AChE for the entire MD simulation (A) and for four equal time intervals (B).

3.2. SASA and secondary structure

The Solvent-Accessible-Surface-Area (SASA) of the Aβ-AChE complex was calculated for every 10 frames in total of 5000 using the LCPO Algorithm (Linear Combinations of Pairwise Overlaps Algorithm) of W e i s e, S h e n k i n and S t i l l [49]. The averaged values of every 100 ns and the convergence of SASA are presented on Fig. 3. For the first 300 ns SASA fluctuates, then it decreases trendily. The decrease in SASA corresponds to more compact complex at the end of MD simulation.
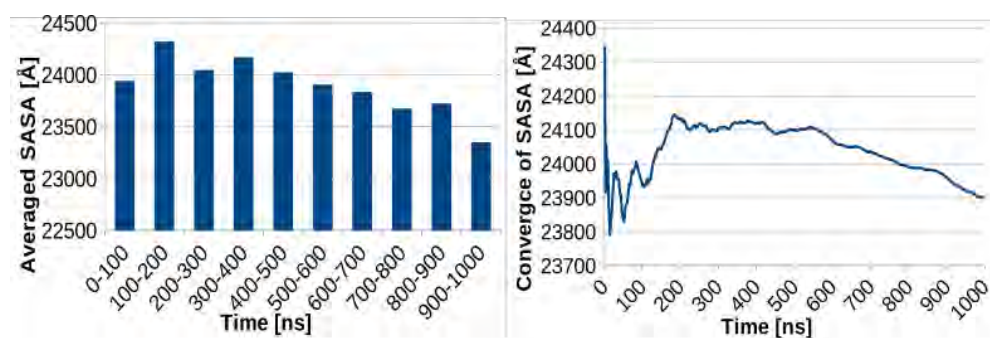
Fig. 3. The averaged (A) and convergence of SASA (B) as function of time

The progression of the secondary structure propensities in Aβ peptide indicates that for the first 50 ns the β-turn is the most common structure, then the helix propensity (including 3-10 helix) dominates till 750 ns, and at the end, helices and

β-turns become equal (Fig. 4). The bend propensity is almost constant during the first half of the simulation, between 500 and 700 ns tends to decrease and during the last 300 ns slightly increases.
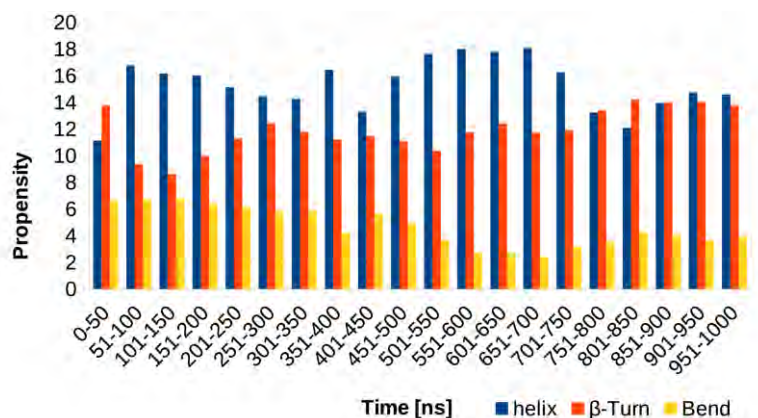
Fig. 4. Propensities of helix, β-turn and bend of Aβ peptide summarized for every 50 ns for 1 μs production dynamics

3.3. Non-native contacts and hydrogen bonds between AChE and Aβ

Native contacts in Amber are defined as those that can be find in a given reference structure or in the first snapshot of the trajectory [50]. All other contacts between pair of atoms within a distance of 7 Å are defined as non-native. The number of contacts of Aβ residues with AChE averaged over 5000 frames is presented in Fig. 5A. There are several Aβ residues acting as anchors. These are the first four residues of the N-terminal (Asp1, Ala2, Glu3 and Phe4) and the pair His14/Gln15 making around and more than 100 contacts each with the enzyme.

The Aβ residues form the highest number of contacts with AChE are Asp1 (133 contacts) and Phe4 (130 contacts), followed by Glu3, His14, Gln15 (above 100 contacts). Ala2 and Glu11 form 93 and 74 contacts with AChE, respectively. The residues Ser26, Arg5, Glu22, Lys28, Val18, Gly9, Asn27, Gly25, Tyr10, Asp23, Phe19, Asp7 and His6 form between 50 and 10 contacts. The remaining Aβ residues form a few or no contact with the enzyme. The number of the intramolecular contacts within the Aβ molecule formed during the production phase is impressive (Fig. 5B). These interactions stabilize the secondary structure of the peptide. The most frequent non-native contacts between Aβ and AChE and within Aβ are presented in Table 1, Appendix. As most frequent contacts are defined those that are formed more than 10 times during the 1000 ns production dynamics. The first four peptide residues – Asp1, Ala2, Glu3 and Phe4 – form contacts with the AChE residues from 344 to 361, while His14 and Gln15 prefer to bind to Leu76, Trp77 and the residues 344-349 (Fig. 1, Appendix). Most of the AChE contact residues correspond to the reported data as they belong to one of the sites on the enzyme surface where Aβ binds [38]. Moreover, new contact residues were found as Pro344, Asp349, Leu353, Ile534, Leu360, Ala361, and Asp372 supplementing the known contacts (Table 1,

146

Appendix). Additionally, one new contact area of AChE interacting with Aβ peptide was found consisting of Leu76 and Trp77. Within the Aβ molecule, the most reactive is His6 forming contacts with 10 Aβ residues followed by Ile31, Phe5 and Met35.
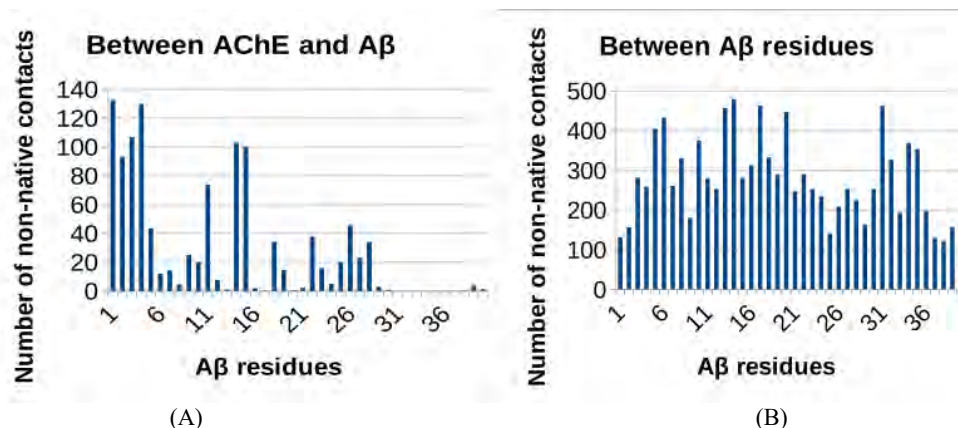
Fig. 5. Number of the non-native contacts between Aβ and AChE (A) and within Aβ (B) summarized over 1000 ns production dynamics.

The total number of the hydrogen bonds formed between Aβ and AChE during the production phase is 164, while those within Aβ are 57 383. This great difference (350 times) is due to the stable secondary structure of Aβ based on multiple hydrogen bonds.

3.4. Water-mediated bridging interactions

A bridging water molecule is one that simultaneously is bound to the Aβ and AChE in at least one of the 5000 frames of production dynamics. We assume that each bridge is a single, continuous interaction and that a given water molecule can form multiple bridging interactions [51]. The number of bridging water molecules and the number of formed bridging interactions for each Aβ residue during the 1 μs MD simulation are presented in Fig. 6. The hydrogen bond cutoffs for distance was 3 Å and for the angle – 135°. As is evident, the number of bridges is greater than the number of bridging molecules. The trajectory processing revealed that thousands water molecules participate in at least one bridging interaction. The most involved Aβ residues in bridging interactions are Glu11, Glu3, Ala2, Asp1, Glu22, Ser26, Lys28, Arg5, Gln15 and His14 with more than 500 interactions (Table 2, Appendix). The vast majority of bridging interactions are short-lasting with duration up to 0.2 ns. The longest-lasting interactions are formed with Gly25 for 2.2, 2.4 and 4.2 ns and they are 41% of the total bridging interactions for this residue, followed by Phe19 with 33%, His14 with 27% and Glu3 with 22%.
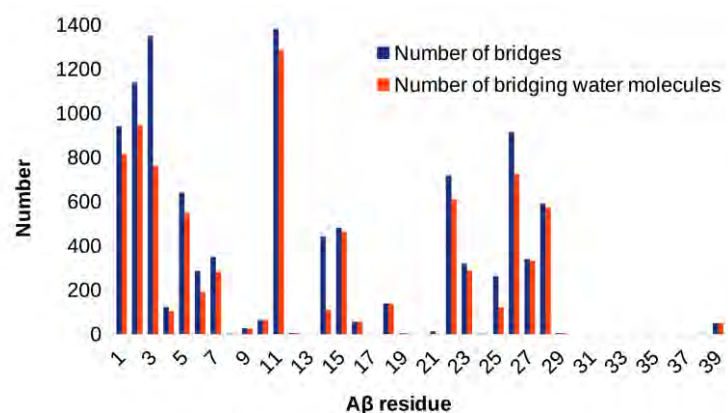
Fig. 6. Number of bridges and bridging water molecules formed between Aβ and AChE during 1000 ns production dynamics

4. Conclusion

The MD simulations of the Aβ-AChE complex performed in the present study revealed that the complex remains stable for 1 µs simulated time with several different modes of binding between the two molecules. The Aβ moves around the PAS and occupies three different areas on the AChE surface. The binding is achieved by hydrogen bonds, π-π stacking and hydrophobic interactions. Most of the hydrogen bonds are mediated by bridging water molecules. The main residence area of Aβ on the surface of AChE is the region 344-361. This region is next to the PAS but far enough to be sterically hindered by dual-site binding AChE inhibitors. The stability of the Aβ-AChE complex is in a good agreement with the experimentally detected AChE molecules in the preamyloid deposits and mature senile plaques. To the best of our knowledge, the present study describes and analyses the longest ever MD simulation of the Aβ-AChE complex.

R e f e r e n c e s

1. K e l l y, J. W. Alternative Conformations of Amyloidogenic Proteins Govern Their Behavior. – Current Opinion in Structural Biology, Vol. **6**, 1996, No 1, pp. 11-17.
2. K o o, E. H., P. T. L a n s b u r y, J. W. K e l l y. Amyloid Diseases: Abnormal Protein Aggregation in Neurodegeneration. – Proceedings of the National Academy of Sciences of the United States of America, Vol. **96**, 1999, No 18, pp. 9989-9990.
3. B a l l a r d, C., S. G a u t h i e r, A. C o r b e t t, C. B r a y n e, D. A a r s l a n d, E. J o n e s. Alzheimer's Disease. – Lancet (London, England), Vol. **377**, 2011, No 9770, pp. 1019-1031.

4. S e l k o e, D. J. Alzheimer's Disease : Genes , Proteins , and Therapy. – Physiological Reviews, Vol. **81**, 2001, No 2, pp. 741-766.
5. G o e d e r t, M., M. G. S p i l l a n t i n i. A Century of Alzheimer's Disease. – Science, Vol. **314**, 2006, No 5800, pp. 777-781.
6. H a r d y, J., D. S e l o k o e. The Amyloid Hypothesis of Alzheimer 's Disease. – Science, Vol. **297**, 2002, No 5580, pp. 353-357.
7. L a z a r o v, O., M. P. D e m a r s. All in the Family: How the Apps Regulate Neurogenesis. – Frontiers in Neuroscience, Vol. **6**, 2012, No JUN, pp. 1-21.
8. K a m e n e t z, F., T. T o m i t a, H. H s i e h, G. S e a b r o o k, D. B o r c h e l t, T. I w a t s u b o, S. S i s o d i a, R. M a l i n o w. APP Processing and Synaptic Function. – Neuron, Vol. **37**, 2003, No 6, pp. 925-937.
9. V a r d y, E. R. L. C., A. J. C a t t o, N. M. H o o p e r. Proteolytic Mechanisms in Amyloid-β Metabolism: Therapeutic Implications for Alzheimer's Disease. – Trends in Molecular Medicine, Vol. **11**, 2005, No 10, pp. 464-472.
10. B e e l, A. J., C. R. S a n d e r s. Substrate Specificity of γ-Secretase and Other Intramembrane Proteases. – Cellular and Molecular Life Sciences, Vol. **65**, 2008, No 9, pp. 1311-1334.
11. J a r r e t t, J. T., E. P. B e r g e r, P. T. L a n s b u r y. The Carboxy Terminus of the Beta Amyloid Protein is Critical for the Seeding of Amyloid Formation: Implications for the Pathogenesis of Alzheimer's Disease. – Biochemistry, Vol. **32**, 1993, No 18, pp. 4693-4697.
12. H a r p e r, J. D., P. T. L a n s b u r y. Models of Amyloid Seeding in Alzheimer's Disease and Scrapie: Mechanistic Truths and Physiological Consequences of the Time-Dependent Solubility of Amyloid Proteins. – Annual Review of Biochemistry, Vol. **66**, 1997, No 1, pp. 385-407.
13. H a r p e r, J. D., C. M. L i e b e r, P. T. L a n s b u r y. Atomic Force Microscopic Imaging of Seeded Fibril Formation and Fibril Branching by the Alzheimer's Disease Amyloid-β Protein. – Chemistry & Biology, Vol. **4**, 1997, No 12, pp. 951-959.
14. S o t o, C., E. M. C a s t a ñ o, B. F r a n g i o n e, N. C. I n e s t r o s a. The -Helical to -Strand Transition in the Amino-Terminal Fragment of the Amyloid -Peptide Modulates Amyloid Formation. – Journal of Biological Chemistry, Vol. **270**, 1995, No 7, pp. 3063-3067.
15. G l a b e, C. G. Structural Classification of Toxic Amyloid Oligomers. – Journal of Biological Chemistry, Vol. **283**, 2008, No 44, pp. 29639-29643.
16. S t r i t t m a t t e r, W. J., A. D. R o s e s. Apolipoprotein E and Alzheimer Disease. – Proceedings of the National Academy of Sciences, Vol. **92**, 1995, No 11, pp. 4725-4727.
17. H o l t z m a n, D. M., K. R. B a l e s, T. T e n k o v a, A. M. F a g a n, M. P a r s a d a n i a n, L. J. S a r t o r i u s, B. M a c k e y, J. O l n e y, D. M c K e e l, D. W o z n i a k, S. M. P a u l. Apolipoprotein E Isoform-Dependent Amyloid Deposition and Neuritic Degeneration in a Mouse Model of Alzheimer's Disease. – Proceedings of the National Academy of Sciences, Vol. **97**, 2000, No 6, pp. 2892-2897.
18. B r o n f m a n, F. C., A. A l v a r e z, C. M o r g a n, N. C. I n e s t r o s a. Laminin Blocks the Assembly of Wild-Type Aβ and the Dutch Variant Peptide into Alzheimer's Fibrils. – Amyloid, Vol. **5**, 1998, No 1, pp. 16-23.
19. N i l s s o n, L. N. G., K. R. B a l e s, G. D i C a r l o, M. N. G o r d o n, D. M o r g a n, S. M. P a u l, H. P o t t e r. α-1-Antichymotrypsin Promotes β-Sheet Amyloid Plaque Deposition in a Transgenic Mouse Model of Alzheimer's Disease. – The Journal of Neuroscience, Vol. **21**, 2001, No 5, pp. 1444-1451.
20. H u g h e s, S. R., O. K h o r k o v a, S. G o y a l, J. K n a e b l e i n, J. H e r o u x, N. G. R i e d e l, S. S a h a s r a b u d h e. 2-Macroglobulin Associates with -Amyloid Peptide and Prevents Fibril Formation. – Proceedings of the National Academy of Sciences, Vol. **95**, 1998, No 6, pp. 3275-3280.
21. T h a m b i s e t t y, M., A. S i m m o n s, L. V e l a y u d h a n, A. H y e et al. Association of Plasma Clusterin Concentration with Severity, Pathology, and Progression in Alzheimer Disease. – Archives of General Psychiatry, Vol. **67**, 2010, No 7, pp. 739-748.
22. S n o w, A. D., R. S e k i g u c h i, D. N o c h l i n, P. F r a s e r, K. K i m a t a, A. M i z u t a n i, M. A r a i, W. A. S c h r e i e r, D. G. M o r g a n. An Important Role of Heparan Sulfate Proteoglycan (Perlecan) in a Model System for the Deposition and Persistence of Fibrillar Aβ-Amyloid in Rat Brain. – Neuron, Vol. **12**, 1994, No 1, pp. 219-234.

23. I n e s t r o s a, N. C., A. A l v a r e z, C. A. P é r e z, R. D. M o r e n o, M. V i c e n t e, C. L i n k e r, O. I. C a s a n u e v a, C. S o t o, J. G a r r i d o. Acetylcholinesterase Accelerates Assembly of Amyloid-β-Peptides into Alzheimer's Fibrils: Possible Role of the Peripheral Site of the Enzyme. – Neuron, Vol. **16**, 1996, No 4, pp. 881-891.

24. R e e s, T. Acetylcholinesterase Promotes Beta-Amyloid Plaques in Cerebral Cortex. – Neurobiology of Aging, Vol. **24**, 2003, No 6, pp. 777-787.

25. S m a l l, D. H., S. M i c h a e l s o n, G. S b e r n a. Non-Classical Actions of Cholinesterases: Role in Cellular Differentiation, Tumorigenesis and Alzheimer's Disease. – Neurochemistry International, Vol. **28**, 1996, No 5-6, pp. 453-483.

26. S o r e q, H., S. S e i d m a n. Acetylcholinesterase – New Roles for an Old Actor. – Nature Reviews Neuroscience, Vol. **2**, 2001, No 4, pp. 294-302.

27. I n e s t r o s a, N. C., A. P e r e l m a n. Distribution and Anchoring of Molecular Forms of Acetylcholinesterase. – Trends in Pharmacological Sciences, Vol. **10**, 1989, No 8, pp. 325-329.

28. F e r n a n d e z, H. L., R. D. M o r e n o, N. C. I n e s t r o s a. Tetrameric (G4) Acetylcholinesterase: Structure, Localization, and Physiological Regulation. – Journal of Neurochemistry, Vol. **66**, 2002, No 4, pp. 1335-1346.

29. C a m p o s, E. O., A. A l v a r e z, N. C. I n e s t r o s a. Brain Acetylcholinesterase Promotes Amyloid-β-Peptide Aggregation But Does Not Hydrolyze Amyloid Precursor Protein Peptides. – Neurochemical Research, Vol. **23**, 1998, No 2, pp. 135-140.

30. M o r á n, M. A., E. J. M u f s o n, P. G ó m e z-R a m o s. Colocalization of Cholinesterases with β-Amyloid Protein in Aged and Alzheimer's Brains. – Acta Neuropathologica, Vol. **85**, 1993, No 4, pp. 362-369.

31. C h a c ó n, M. A., A. E. R e y e s, N. C. I n e s t r o s a. Acetylcholinesterase Induces Neuronal Cell Loss, Astrocyte Hypertrophy and Behavioral Deficits in Mammalian Hippocampus. – Journal of Neurochemistry, Vol. **87**, 2003, No 1, pp. 195-204.

32. I n e s t r o s a, N. C., A. A l v a r e z, J. G a r r i d o, F. C a l d e r ó n, F. C. B r o n f m a n, F. D a j a s, M. K. G e n t r y, B. P. D o c t o r. Acetylcholinesterase Promotes Alzheimer's β-Amyloid Fibril Formation. – In: Alzheimer's Disease: Biology, Diagnosis and Therapeutics. Vol. **1997**. Chichester, Wiley, 1997, pp. 499-508.

33. R e y e s, A. E., M. A. C h a c ó n, M. C. D i n a m a r c a, W. C e r p a, C. M o r g a n, N. C. I n e s t r o s a. Acetylcholinesterase-Aβ Complexes are More Toxic Than Aβ Fibrils in Rat Hippocampus. – The American Journal of Pathology, Vol. **164**, 2004, No 6, pp. 2163-2174.

34. B o l o g n e s i, M. L., A. M i n a r i n i, M. R o s i n i, V. T u m i a t t i, C. M e l c h i o r r e. From Dual Binding Site Acetylcholinesterase Inhibitors to Multi-Target-Directed Ligands (MTDLs): A Step Forward in the Treatment of Alzheimers Disease. – Mini-Reviews in Medicinal Chemistry, Vol. **8**, 2008, No 10, pp. 960-967.

35. D e F e r r a r i, G. V., M. A. C a n a l e s, I. S h i n, L. M. W e i n e r, I. S i l m a n, N. C. I n e s t r o s a. A Structural Motif of Acetylcholinesterase That Promotes Amyloid β-Peptide Fibril Formation. – Biochemistry, Vol. **40**, 2001, No 35, pp. 10447-10457.

36. H o u, L.-N., J.-R. X u, Q.-N. Z h a o, X.-L. G a o, Y.-Y. C u i, J. X u, H. W a n g, H.-Z. C h e n. A New Motif in the N-Terminal of Acetylcholinesterase Triggers Amyloid-β Aggregation and Deposition. – CNS Neuroscience & Therapeutics, Vol. **20**, 2014, No 1, pp. 59-66.

37. M i s h r a, P., S. R. A y y a n n a n, G. P a n d a. Perspectives on Inhibiting β-Amyloid Aggregation through Structure-Based Drug Design. – ChemMedChem, Vol. **10**, 2015, No 9, pp. 1467-1474.

38. L u s h c h e k i n a, S. V., E. D. K o t s, D. A. N o v i c h k o v a, K. A. P e t r o v, P. M a s s o n. Role of Acetylcholinesterase in β-Amyloid Aggregation Studied by Accelerated Molecular Dynamics. – BioNanoScience, Vol. **7**, 2017, No 2, pp. 396-402.

39. C h e u n g, J., M. J. R u d o l p h, F. B u r s h t e y n, M. S. C a s s i d y, E. N. G a r y, J. L o v e, M. C. F r a n k l i n, J. J. H e i g h t. Structures of Human Acetylcholinesterase in Complex with Pharmacologically Important Ligands. – Journal of Medicinal Chemistry, Vol. **55**, 2012, No 22, pp. 10282-10286.

40. S t i c h t, H., P. B a y e r, D. W i l l b o l d, S. D a m e s, C. H i l b i c h, K. B e y r e u t h e r, R. W. F r a n k, P. R o s c h. Structure of Amyloid A4-(1-40)-Peptide of Alzheimer's Disease. – European Journal of Biochemistry, Vol. **233**, 1995, No 1, pp. 293-298.

41. L y s k o v, S., J. J. G r a y. The RosettaDock Server for Local Protein-Protein Docking. – Nucleic Acids Research, Vol. **36** (Web Server issue), 2008, pp. W233-W238.

42. W a n g, J., R. M. W o l f, J. W. C a l d w e l l, P. A. K o l l m a n, D. A. C a s e. Development and Testing of a General Amber Force Field. – Journal of Computational Chemistry, Vol. **25**, 2004, No 9, pp. 1157-1174.

43. A d e l m a n, S. A., J. D. D o l l. Generalized Langevin Equation Approach for Atom/Solid Surface Scattering: Collinear Atom/Harmonic Chain Model. – The Journal of Chemical Physics, Vol. **61**, 1974, No 10, pp. 4242-4245.

44. B e r e n d s e n, H. J. C., J. P. M. P o s t m a, W. F. van G u n s t e r e n, A. D i N o l a, J. R. H a a k. Molecular Dynamics with Coupling to an External Bath. – The Journal of Chemical Physics, Vol. **81**, 1984, No 8, pp. 3684-3690.

45. M a i e r, J. A., C. M a r t i n e z, K. K a s a v a j h a l a, L. W i c k s t r o m, K. E. H a u s e r, C. S i m m e r l i n g. Ff14SB: Improving the Accuracy of Protein Side Chain and Backbone Parameters from Ff99SB. – Journal of Chemical Theory and Computation, Vol. **11**, 2015, No 8, pp. 3696-3713.

46. D a r d e n, T., D. Y o r k, L. P e d e r s e n. Particle Mesh Ewald: An Nlog(N) Method for Ewald Sums in Large Systems. – The Journal of Chemical Physics, Vol. **98**, 1993, No 12, pp. 10089-10092.

47. C i c c o t t i, G., J. P. R y c k a e r t. Molecular Dynamics Simulation of Rigid Molecules. – Computer Physics Reports, Vol. **4**, 1986, No 6, pp. 346-392.

48. R o e, D. R., T. E. C h e a t h a m. PTRAJ and CPPTRAJ: Software for Processing and Analysis of Molecular Dynamics Trajectory Data. – Journal of Chemical Theory And Computation, Vol. **9**, 2013, No 7, pp. 3084-3095.

49. W e i s e r, J., P. S. S h e n k i n, W. C. S t i l l. Approximate Atomic Surfaces From Linear Combinations of Pairwise Overlaps (LCPO). – Journal of Computational Chemistry, Vol. **20**, 1999, No 2, pp. 217-230.

50. C a s e, D. A., I. Y. B e n-S h a l o m, S. R. B r o z e l l, D. S. C e r u t t i et al. Amber 2018. Reference Manual. Vol. **2018**. San Francisco, University of California.

51. I v a n o v, S. M., I. D i m i t r o v, I. A. D o y t c h i n o v a. Bridging Solvent Molecules Mediate RNase A – Ligand Binding. – PLoS ONE, Vol. 14, **2019**, No 10, pp. 1-23.

Appendix
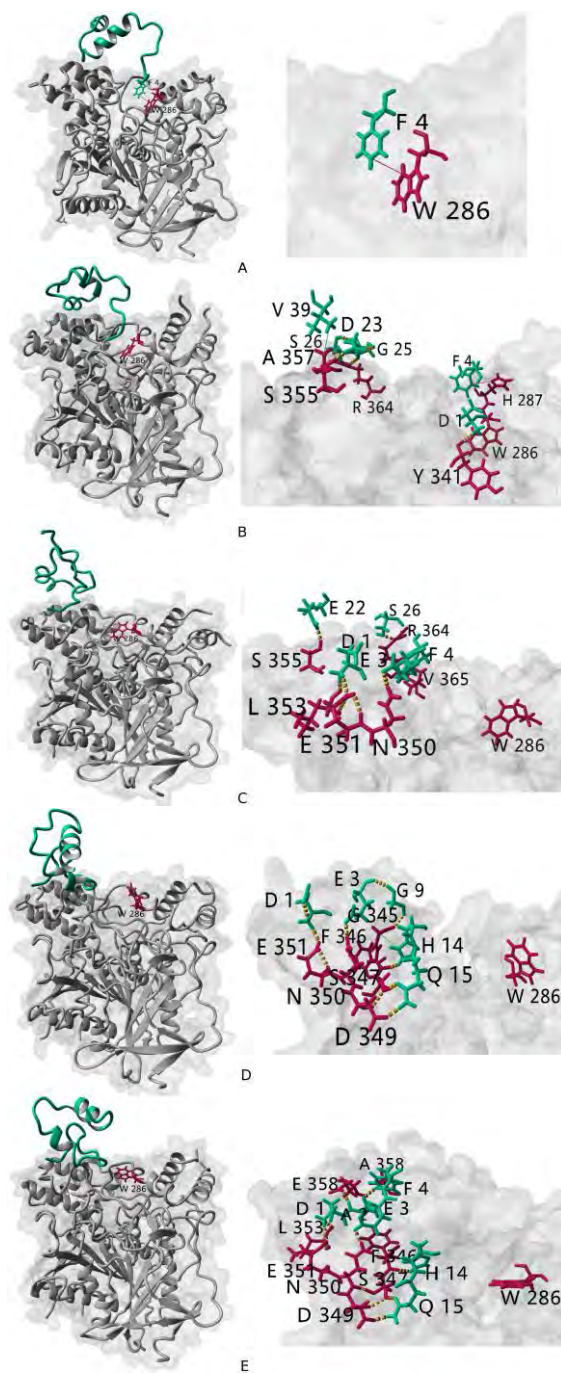
Fig. 1. The AChE-Aβ complex best scored by RosettaDock (A); the AChE-Aβ complex at 88.6 ns of simulation (B); at 418.8 ns (C); at 525.8 ns (D); at 711.4 ns (E). The π-π stacking is shown by red line. The hydrogen bonds are presented by yellow dashes and the hydrophobic contacts – by green lines. The AChE residues are coloured in red, the Aβ residues – in green

Table 1. The most frequent non-native contacts (over 10 contacts) between Aβ
and AChE and within Aβ

Aβ res	AChE contact residues	Aβ contact residues
D1	N350, E351, S352, L353, I354, E358	E22
A2	F346, L353, I354, E358	-
E3	P344, G345, F346, N350, E351	V18
F4	P344, G345, F346, E358, A361	-
R5	E358	H14, E22
H6	-	H14, A21, E22, G25, S26, N27, K28, A30, I31, I32
D7	-	K28, I31
S8	-	H14, L17, V18, I31
G9	P344	E3
Y10	P344	M35
E11	E292, P344	-
H13	-	I31, L34, M35
H14	L76, P344, G345, F346, S347	R5, H6, S8
Q15	L76, W77, S347, D349	-
K16	-	V39
L17	-	S8, I31, L34, M35
V18	D349, N350	E3, S8
F20	-	S26, I31, L34, M35, V39
A21	-	R5, H6, I31
E22	-	D1, R5, H6
V24	-	A30
G25	-	H6
S26	L360	H6, F20
N27	-	H6
K28	R364, D372	H6, D7
A30	-	H6, V24
I31	-	H6, D7, S8, H13, L17, F20, A21
L34	-	H13, F20
M35	-	W10, H13, K16, L17, F20

Table 2. Life-times of the bridging interactions for each Aβ residue

Aβ residue	Short-lasting ($\leq$ 0.2 ns)	Long-lasting ($>$ 0.2 ns)	% long-lasting
D1	863	77	8.19
A2	936	203	17.82
E3	1046	303	22.46
F3	115	8	6.50
R5	550	90	14.06
H6	240	45	15.79
D7	279	70	20.06
S8	2	0	0
G9	26	0	0
Y10	63	0	0
E11	1294	88	6.37
V12	4	0	0
H14	320	121	27.44
Q15	465	16	3.33
K16	54	1	1.82
V18	136	3	2.16
F19	2	1	33.33
A21	6	6	50
E22	624	94	13.09
D23	279	40	12.54
V24	2	0	0
G25	155	107	40.84
S26	769	144	15.77
N27	335	4	1.18
K28	564	26	4.41
G29	4	0	0
G38	1	0	0
V39	44	5	10.20